

Kinetic Analysis of Isobutane/Butene Alkylation over Ultrastable H–Y Zeolite

Michael F. Simpson,[†] James Wei, and Sankaran Sundaresan*

Department of Chemical Engineering, Princeton University, Princeton, New Jersey 08544

The alkylation of isobutane with *trans*-2-butene over ultrastable Y-type zeolites has been studied. It is well-known that this reaction is accompanied by a rapid deactivation of the catalyst. The objective of our study is to elucidate the route to catalyst deactivation so that the means of mitigating this problem can be identified. Using the initial reaction rate data, evidence has been found for a Brønsted acid mechanism. Under liquid-phase conditions, the reaction has been found to be severely diffusion limited. Using a kinetic model that accounts for the effect of diffusion, it was found that alkylation over this catalyst suffers from slow hydride transfer relative to olefin addition. This gives rise to a rapid formation of C₁₂⁺ carbocations. The formation of these cations has been tied to catalyst deactivation, using a mathematical model for the reaction. On the basis of the insight gained from the experiments and modeling work, optimal reactor and catalyst design issues are examined. It is inferred from the reaction mechanism and confirmed experimentally that alkylation under pulsed flow conditions yields higher trimethylpentane/dimethylhexane ratios and slower rates of deactivation. It is suggested that the cause of the slow rate of hydride transfer is steric hindrance. Strategies for relieving this steric hindrance are proposed.

Introduction

In the coming years, the reformulation of gasoline mandated in this country by the Clean Air Act (1990) will require a decrease in the utilization of olefins and aromatics and an increase in the demand for highly branched paraffinic molecules, such as trimethylpentanes. The primary source of these branched paraffins is the alkylation of isobutane with normal C₃–C₅ olefins.

This alkylation reaction is currently catalyzed using either hydrofluoric acid (HF) or sulfuric acid (H₂SO₄) in petroleum refineries (Albright, 1977; Grayson, 1978). In the case of the reaction of isobutane with butene, the main products are trimethylpentanes (TMP) and dimethylhexanes (DMH). The TMP's are the more desirable products due to their higher octane numbers (Rose and Cooper, 1977). Though the liquid acids rapidly catalyze the alkylation reaction even at subambient temperatures, there are multiple drawbacks involved with using them. Conjunct polymerization occurs rapidly when using H₂SO₄, resulting in a sludge byproduct containing both heavy hydrocarbons and spent acid (Pines, 1981). This sludge must then be sent to a separate regenerating plant to recover and recycle the acid. The primary problem with using HF pertains to safety, as HF leaks are particularly difficult to contain due to the acid's high volatility (Albright, 1990; Fthenakis, 1993). There are also economic advantages to replacing the liquid acid catalysts. The current cost of alkylation catalysts accounts for about 30% of the total catalyst cost in petroleum refining (Corma and Martinez, 1993). The rate of catalyst consumption for H₂SO₄ alkylation, for instance, is 2 orders of magnitude (by weight) higher than for catalytic cracking, which is catalyzed by zeolitic solid acids (Corma and Martinez, 1993). So, it can be seen that there is potential to reduce the amount of catalyst needed for alkylation and, thus, the operating cost by switching from a liquid to a solid acid. The benign nature of the solid acids also makes them attractive for use as alkylation catalysts.

It was shown by Kirsch et al. (1972) that H–Y and rare-earth-exchanged Y zeolite (RE-Y) are both active toward this reaction. Since then, alkylation of isobutane with butenes over a number of zeolitic and non-zeolitic solid acids has been described in the literature (McClure and Brandenberger, 1977; Weitkamp, 1980; Chu and Chester, 1986; Weitkamp and Jacobs, 1993; Corma et al., 1994a–d; Guo et al. 1994a,b; Okuhara et al., 1994; Stöcker et al., 1994). A detailed discussion of much of the published work in this area is available in a review article by Corma and Martinez (1993).

Unfortunately, zeolites and other solid acids deactivate rapidly during alkylation (Weitkamp, 1980; Chu and Chester, 1986; Weitkamp and Maixner, 1987; Corma et al., 1994a–d). This deactivation renders the solid-acid-based alkylation process economically unattractive. The cost of regenerating the solid acid in such a process is estimated to be prohibitively high. Though several researchers have studied isobutane/butene alkylation over solid acids, no effort has been forward to separate the intrinsic kinetics from the catalyst deactivation characteristics. In the present study, we have examined in detail the kinetics of isobutane/olefin alkylation over ultrastable H–Y (Si/Al = 6.9) zeolite as a model system in an effort to elucidate the route to catalyst deactivation.

Armed with this knowledge, one can examine whether the problem of catalyst deactivation can be mitigated by judicious choice of reactor geometry and operating conditions. More importantly, a definitive understanding of the rate-determining step and deactivation route may also guide the development of new catalysts that are more resistant to deactivation. This is particularly valuable, as the approach in the past appears to have been one where researchers have simply screened every known solid acid for its alkylation activity. Indeed, all of the known solid acids have been patented by one or more companies, yet no viable process has emerged. Thus, it appears that new solid acids must be specially designed for the alkylation reaction. Exactly what new properties must be endowed on such a catalyst is not

[†] Presently at Technology Development Division, Argonne National Laboratory, P.O. Box 2528, Idaho Falls, ID 83403.

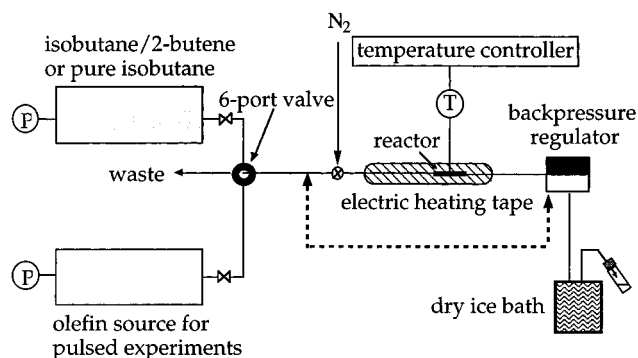


Figure 1. Alkylation reactor schematic. Dashed line represents optional placement of backpressure regulator. On-line sampling system is not pictured here.

clear, and the intent of this paper is to shed some light on this issue.

Experiments

Catalyst. Ultrastable Y-type faujasite with a Si/Al ratio of 6.9 extruded into pellets with approximately 20% inorganic binder was obtained from Union Carbide (LZY-84) and calcined at 673 K prior to use as the H form of ultrastable Y, USHY. The catalyst was crushed and sieved to a variety of particle sizes with average diameters ranging from 91 to 231 μm .

Kinetic Experiments. A microreactor constructed entirely of stainless steel was used to carry out the kinetic experiments (see Figure 1). The unit consists of a 2-in.-long tube (0.055-in. i.d. $\frac{1}{8}$ -in. o.d.) packed with 2–50 mg of catalyst, a high-pressure syringe pump (Isco), and a dome-type backpressure regulator (Grove). For experiments with constant feed composition, a feed mixture of desired composition was prepared by mixing either *trans*-2-butene (Aldrich, 99+%) or 5% *trans*-2-butene/95% isobutane mixture (Scott Specialty Gases) with isobutane (Matheson, 99+%). In either case, the as-received liquified gases were passed over a bed of dehydrated alumina prior to loading the syringe pumps. This purification step was included to minimize the concentrations of oxygenates in the feed. For pulse experiments, isobutane was delivered at a steady rate by the syringe pump, and a known volume of olefin was injected into the reactor through a sampling valve (see Figure 1). Pulse experiments were performed with *trans*-2-butene, 1-butene (Aldrich, 99+%), propene (Aldrich, 99+%), and *trans*-2-pentene (Aldrich, 99+%). The backpressure regulator (BPR) was always set at 300 psig, thus maintaining the fluid upstream of the reactor under liquid-phase conditions. The dashed line in Figure 1 represents two different locations for the BPR. Placing it in the downstream location shown in the figure permits kinetic experiments in a liquid phase. By moving the BPR upstream of the reactor, vapor-phase experiments can be performed.

The reactor effluent was condensed into a liquid phase by passing it through a dry ice chilled coil, and samples were collected directly into vials. These vials were kept cold via immersion in a dry ice bath (methanol or acetone/dry ice), thus maintaining the vapor pressure of the samples low. Fractions of each sample (ca. 1 μL) were transferred manually from the vials to the gas chromatograph using chilled, insulated syringes. Repeated injection of given samples indicated that they can be stored for several hours without a noticeable change in their compositions. The gas chromatograph

was equipped with a flame ionization detector and a 100-m fused silica capillary column specially designed for separating alkylates (Supelco, Petrocol DH). The isobutane supply contained approximately 4200 ppm of *n*-butane as a principal impurity, and this was used as an internal standard. Although *n*-butane is formed during alkylation, the amount formed in our experiments is negligible compared to the quantity in the feed. The legitimacy of choosing this standard was verified by comparing the chromatography peaks for *n*-butane to both propane and 2,2-dimethylbutane. Propane was present as an impurity in the isobutane supply, and measured quantities of 2,2-dimethylbutane were added to several of the feed mixtures as an additional internal standard. (It was found in preliminary experiments that 2,2-dimethylbutane was not formed during alkylation over faujasites.) The ratio of the integrated areas for these peaks remained essentially constant for all of the experiments described in this paper.

For the sake of analyzing deactivation rates, an on-line sampling system was assembled. This was necessary since the BPR was found to mask the true rate of deactivation. The number of experiments performed using this mode of sampling was severely limited, however, since the sampling valve developed some alignment problems and also introduced large pressure fluctuations in the reactor. Since it was found that the time-zero results are not affected by the sampling method, the time-zero kinetics analysis relied only upon results obtained using the manual sampling system.

Unless noted otherwise, catalyst samples were activated in situ by ramping the reactor temperature to 523 K at a rate of 2 $^{\circ}\text{C}/\text{min}$ and holding it at this temperature for 10 h. Ultrahigh-purity nitrogen (Scott Specialty Gases, 99.9995%), further purified using Drierite and Oxy-Purge-N oxygen trap (Alltech), was flowed over the catalyst at 30 mL/min during catalyst activation. For liquid-phase kinetic experiments, the reactor was prepressurized with this ultrahigh-purity nitrogen to 300 psig before initiating flow of reactor feed. Reactor dead time was determined by observing the breakthrough of liquid out of the dry ice bath.

Results and Discussion

A well-known feature of solid-acid-catalyzed alkylation is the steady, and frequently rapid, decline of catalytic activity. When kinetic experiments were attempted with fairly low feed I/O ratios in the range of 5–15, which are typical of industrial liquid-acid-catalyzed alkylation, the catalyst deactivated within a few seconds, rendering quantitative analysis of the results essentially impossible. The rate of catalyst deactivation was found to decrease as the concentration of olefin in the feed was decreased. With sufficiently dilute feeds (I/O ratios in the range of 500–3500), it was possible to obtain in a reproducible manner experimental data on butene conversion and product selectivity, which can be used to analyze both reaction mechanism and kinetics. Consequently, the focus has been upon experiments with highly dilute feeds.

Table 1 summarizes the alkylate product distribution obtained in a representative liquid-phase alkylation experiment using isobutane and *trans*-2-butene as reactants. The product distribution is affected by the feed composition, weight hourly space velocity (WHSV, grams of feed per gram of catalyst per hour), catalyst characteristics, and time on stream (TOS). In addition to the products listed in Table 1, 1-butene, *trans*-2-

Table 1. Typical Alkylation Product Distributions^a

product	mol % at TOS of		
	0.1 min	1.0 min	1.6 min
isopentane	10.0	7.2	7.8
2,3-dimethylbutane	3.9	3.1	3.2
2-methylpentane	0.9	0.7	0.9
3-methylpentane	0.7	0.6	0.7
total of C ₆ 's	5.5	4.4	4.8
2,4-dimethylpentane	4.7	3.9	4.1
2,3-dimethylpentane	1.7	1.7	1.8
total of C ₇ 's	6.4	5.6	5.9
2,2,4-trimethylpentane	17.8	16.9	16.6
2,5-dimethylhexane	0.8	0.8	0.6
2,4-dimethylhexane	5.0	5.2	5.1
2,3,4-trimethylpentane	25.2	27.3	26.3
2,3,3-trimethylpentane	21.2	23.6	23.0
2,3-dimethylhexane	3.7	4.0	3.8
3,4-dimethylhexane	0.7	0.9	1.3
total of C ₈ 's	74.4	78.7	76.7
2,2,5-trimethylhexane	0.0	0.3	0.3
2,6-dimethylheptane	3.6	2.8	3.5
total of C ₉ 's	3.6	3.1	3.8
others	0.1	1.0	1.0
TMP/DMH	6.3	6.2	6.1
molar yield ^b	0.76	1.1	1.0
mass yield ^c	1.5	2.2	2.0

^a USHY, $d_p = 231 \mu\text{m}$, WHSV = 12 000 h⁻¹, (I/O)₀ = 820, $T_{\text{rxn}} = 373 \text{ K}$, $T_{\text{act}} = 523 \text{ K}$, liquid phase. ^b Molar yield = moles of products per mole of butene consumed. ^c Mass yield = grams of products per gram of butene consumed.

butene, and *cis*-2-butene were also observed in the reactor effluent. All the isomers of butene were lumped together for the purpose of calculating fractional conversion of butene. It can be readily argued from the reaction stoichiometry that the total number of moles of various alkanes formed should add up to the total number of moles of butene reacted, provided no alkenes or carbonaceous deposit is formed. In a transient experiment of the type performed in our studies, the rate of production of a product in the reactor will inevitably be different from the rate at which it appears in the effluent. Therefore, the ratio of the molar yield of products in the effluent stream at any instant of time to the number of moles of butenes consumed (or retained) in the reactor will vary with time even in the absence of catalyst deactivation. In particular, as a result of product accumulation inside the catalyst pellets, this ratio will be small in the beginning and will often increase with time to some asymptotic value. This is illustrated in Table 1, where it is seen that this ratio is 0.76 at TOS = 0.1 min and it rises to a value of around unity after a minute.

Butene conversion decreased with time on stream, as illustrated in Figure 2. The rate at which butene conversion decreases is influenced by feed concentration of olefin, WHSV, and reaction temperature. In order to perform a quantitative analysis of alkylation kinetics over fresh catalysts, the time-dependent data such as that shown in Figure 2 were extrapolated to zero time. The concentrations of the individual products in the effluent stream were also extrapolated to obtain time-zero values, which were then used as measures of alkylation characteristics of fresh catalyst.

Effect of Diffusion. In order to assess the role of transport limitation on the observed catalytic activity of USHY, kinetic experiments were performed with particles of different sizes and contact times, τ_v (defined here as volume of catalyst divided by the volumetric flow rate of the feed mixture). As discussed elsewhere in greater detail (Simpson et al., 1996), alkylation under

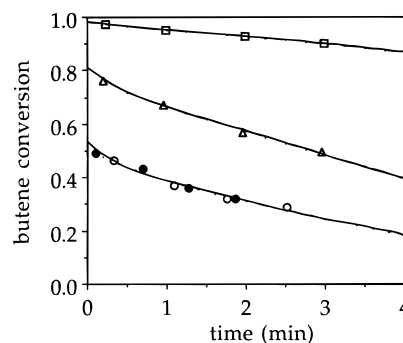


Figure 2. Time-dependent butene conversion at 6300 h⁻¹ (□), 14 000 h⁻¹ (△), and 25 000 h⁻¹ (●, ○) (USHY, $d_p = 231 \mu\text{m}$, (I/O)₀ ≈ 830, $T_{\text{rxn}} = 373 \text{ K}$, $T_{\text{act}} = 523 \text{ K}$, liquid phase).

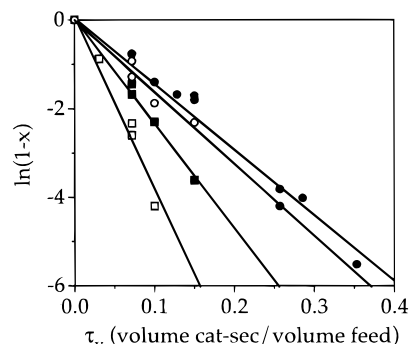


Figure 3. Kinetic plots for USHY-catalyzed alkylation for particle sizes of 91 μm (□), 143 μm (■), 196 μm (○), and 231 μm (●) ((I/O)₀ ≈ 1000, $T_{\text{rxn}} = 373 \text{ K}$, $T_{\text{act}} = 523 \text{ K}$, liquid phase).

liquid-phase conditions was found to be severely limited by intraparticle diffusion. (Note that it was determined that the rate of alkylation was not affected by external mass transfer, by running experiments at different total flow rates but identical WHSV's. The time-zero butene conversions obtained in all of these experiments were nearly identical, indicating the absence of any external mass-transfer resistance (Simpson, 1996).) The effect of intraparticle diffusional resistance is illustrated in Figure 3, showing time-zero butene conversion as a function of contact time for different particle sizes. A preliminary analysis of diffusional limitation was performed assuming that the experimental unit can be modeled as a plug flow reactor and that alkylation is pseudo-first-order in butene concentration. The solid lines in Figure 3 correspond to $x = 1 - \exp(-k_{\text{app}}\tau_v)$ where the apparent rate constant is given by k_{app} (volume of feed/volume catalyst·second) = $2200/d_p$ (μm). The inverse dependence of k_{app} on particle diameter implies intraparticle diffusion control, and this can be confirmed through a Weisz–Prater analysis (Simpson et al., 1996). The Weisz–Prater (1954) analysis requires a knowledge of the diffusivity, D , of butene in the catalyst pellet, which was not measured in our work. It is, however, reasonable to anticipate D to be in the range of 10^{-11} – $10^{-9} \text{ m}^2/\text{s}$. Taking D to be $10^{-10} \text{ m}^2/\text{s}$, the Weisz–Prater number, $\eta\phi^2 = k_{\text{app}}d_p^2/36D$, was found to be 44 for the 91- μm particles at 373 K, which is much larger than the threshold value of unity.

It is generally difficult to study the mechanism and intrinsic kinetics when the reaction is so severely limited by diffusion. Therefore, we explored the means of mitigating this problem. We first considered the effect of lowering the reaction temperature. At fixed feed composition and WHSV, butene conversion decreased as the temperature was lowered; see Table 2. However, the Weisz–Prater number remained ap-

Table 2. Effect of Lowering the Reaction Temperature on the Time-Zero Conversion, TMP/DMH Ratio, and Weisz–Prater Number^a

<i>T</i> , K	<i>x</i>	(TMP/DMH) ₀	$\eta\phi^2$
273	0.533	7.9	43
303	0.736	9.2	75
333	0.817	8.6	96
373	0.900	6.5	130

^a USHY, $d_p = 143 \mu\text{m}$, WHSV = 18 000 h⁻¹, (I/O)₀ = 1250, $T_{\text{act}} = 523 \text{ K}$, liquid phase, $D = 10^{-10} \text{ m}^2/\text{s}$ (assumed).

precipably larger than unity over the entire temperature range studied (Table 2). Assuming that the diffusivity does not change appreciably with temperature and that the observed first-order rate constant behaves according to a simple Arrhenius law, it can be estimated that the reaction temperature would have to be lowered to less than 160 K in order for the Weisz–Prater number to become less than unity for a particle diameter of 91 μm ! In principle, intraparticle diffusional limitation can be overcome by decreasing the particle size further. However, this was not practical in our experimental reactor. Finally, the effect of diffusion can be mitigated by increasing the intraparticle diffusion coefficient, D . Such an increase in the diffusivity can be achieved by carrying out the alkylation under vapor-phase conditions, instead of liquid-phase conditions. Note that the catalyst pellets were comprised of many zeolitic crystals bound loosely together by an inorganic binder. The rate-limiting diffusional process, referred to above, occurs in the large mesopores surrounding the crystals, where transport occurs via bulk diffusion. Bulk diffusivities for the vapor phase are, of course, much larger than those in the liquid phase. This consideration led us to try vapor-phase experiments as a means of overcoming the diffusional disguise of intrinsic kinetics.

Vapor-Phase Alkylation Experiments. The Weisz–Prater number for vapor-phase experiments at 373 K was experimentally found to be 0.5 for the 143- μm particles (assuming a value of $10^{-6} \text{ m}^2/\text{s}$ for D). Typical product distributions obtained in vapor-phase experiments are illustrated in Table 3. The two columns of data correspond to experiments performed at 373 and 303 K. A comparison of these product distributions with those shown earlier for alkylation under liquid-phase conditions reveals that, under vapor-phase conditions, selectivity toward C₅–C₇ compounds is appreciably higher, while C₈ selectivity and the TMP/DMH ratio are lower at a given temperature. However, it appears likely that by lowering the reaction temperature sufficiently, the selectivity for vapor-phase experiments may be made to approach that of the liquid-phase experiments. Unfortunately, the low temperatures required to verify this hypothesis could not be achieved with our current experimental setup.

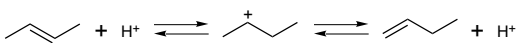

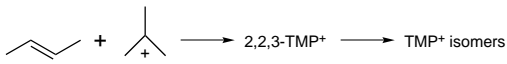
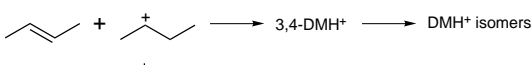
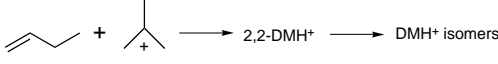
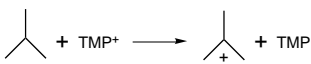
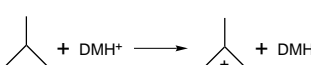
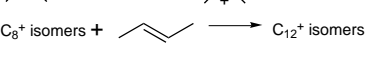

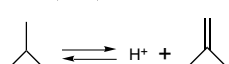
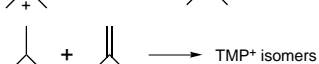
Alkylation Mechanism. No reaction products were observed when USHY activated at 523 K was contacted with a feed containing only isobutane. Thus, the initiation of alkylation over USHY occurs through a step involving an olefin, which is typical of catalysis by Brønsted acid sites. The set of initiation reactions presented in Table 4 is well established in alkylation catalyzed by HF and H₂SO₄ (Pines, 1981). Accordingly, 2-butene combines with a proton yielding a *sec*-butyl cation, which can either give up a proton forming 2-butene or 1-butene (reaction R1), or abstract a hydride ion from isobutane forming *n*-butane and a *tert*-butyl cation (reaction R2). The applicability of this initiation sequence for the USHY catalyst can be verified, at least

Table 3. Product Distribution for Vapor-Phase Experiments^a

product	mol %	
	$T_{\text{rxn}} = 373 \text{ K}$	$T_{\text{rxn}} = 303 \text{ K}$
isopentane	14.0	21.3
2,3-dimethylbutane	18.1	8.1
2-methylpentane	5.3	1.9
3-methylpentane	2.8	2.6
total of C ₆ 's	26.2	12.6
2,4-dimethylpentane	12.4	6.3
2,3-dimethylpentane	4.8	4.5
total of C ₇ 's	17.2	10.8
2,2,4-trimethylpentane	18.6	14.9
2,5-dimethylhexane	2.1	0.4
2,4-dimethylhexane	5.5	3.6
2,3,4-trimethylpentane	4.4	14.7
2,3,3-trimethylpentane	6.8	19.8
2,3-dimethylhexane	1.6	0.8
3,4-dimethylhexane	0.6	0.4
total of C ₈ 's	39.6	54.6
2,2,5-trimethylhexane	0.4	0.2
2,6-dimethylheptane	0.0	0.0
total of C ₉ 's	0.4	0.2
others	2.6	0.5
TMP/DMH	3.1	9.6
molar yield ^b	0.78	0.46
mass yield ^c	1.4	0.82

^a USHY, $d_p = 143 \mu\text{m}$, WHSV = 3100–4200 h⁻¹, (I/O)₀ ≈ 860, $T_{\text{act}} = 523 \text{ K}$, TOS ≈ 0.3 min. ^b Molar yield = moles of products per mole of butene consumed. ^c Mass yield = grams of products per gram of butene consumed.

Table 4. Mechanism for Isobutane/Butene Alkylation over USHY

reaction	no.
	R1
	R2
	R3
	R4
	R5
	R6
	R7
	R8
$\text{C}_{12}^+ \text{ isomers} \longrightarrow \text{C}_x^+ + \text{C}_{12-x} \quad x = 2, 3, 4, 5, \dots$	R9
	R10
	R11
	R12

qualitatively, in two ways; first, by studying the effect of activation temperature on the rate of alkylation and, second, by looking for *n*-butane in the alkylation products.

It has been shown by Ward (1967) that the temperature of activation determines the concentration of Brønsted and Lewis acid sites in a H–Y zeolite. His data on the relative number of Brønsted acid sites as a

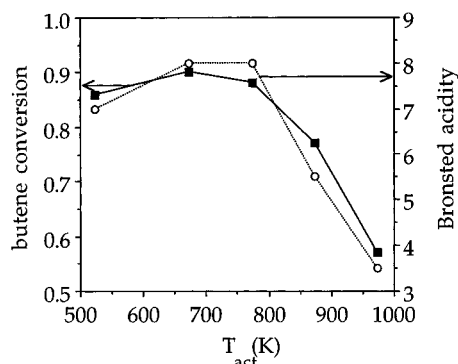


Figure 4. Effect of activation temperature on time-zero conversions (■) (USHY, $d_p = 196 \mu\text{m}$, WHSV = 3100 h^{-1} , $(\text{I/O})_0 = 870$, $T_{\text{rxn}} = 373 \text{ K}$, vapor phase) and Brønsted acidity (○) (data from Ward (1967)).

function of activation temperature as well as our data on time-zero butene conversion under vapor-phase conditions is shown in Figure 4. The acid site concentrations were measured by Ward (1967) using in situ infrared spectroscopy of pyridine adsorbed onto the zeolite surface. The relative number of Brønsted acid sites is defined in this case as the ratio of the spectral absorption associated with the protonated pyridine divided by the mass of the catalyst sample. The concentration of Brønsted acid sites increases at first with activation temperature; however, at higher activation temperatures, it decreases as a result of conversion of the Brønsted sites into Lewis sites (Gates, 1992). The time-zero conversion data given were measured at fixed particle size, feed composition, reaction temperature, and WHSV. The close correspondence between the relative number of Brønsted acid sites and butene conversion seen in Figure 4 is striking, confirming that alkylation over USHY is catalyzed by Brønsted acid sites. (It should be remarked that such a linear relation can be expected only if the reaction is not severely limited by diffusion. It is for this specific reason that these experiments were performed under vapor-phase conditions.)

The appearance of a small amount of *n*-butane in the product mixture (at least initially) has been noted in previous studies (Corma and Martinez, 1993). The presence of *n*-butane in the feed as an impurity at a fairly high concentration (ca. 4200 ppm) makes it impossible to detect in our experiments whether or not any *n*-butane is being formed in the reaction. To circumvent this problem, we studied alkylation of isobutane with *trans*-2-pentene, which should yield *n*-pentane as an initial product if the proposed initiation sequence is correct. This experiment was performed in a pulse-mode and liquid-phase condition, where a steady isobutane flow was maintained and a *trans*-2-pentene pulse of known volume was injected into the reactor. Samples of reactor effluent were gathered at various times and analyzed. The results were then integrated to calculate cumulative yields, which are summarized in Table 5. The *n*-butane and isobutane formed in this pulse experiment, if they were formed at all, could not be detected due to their presence in the feed in relatively large excess. *n*-Pentane was, indeed, observed in the products from the *trans*-2-pentene pulse experiment, lending additional support for the mechanism. The other products listed in this table will be discussed later.

Note that the initiation steps in Table 4 include isomerization reactions. Figure 5 shows the initial 1-butene concentration in the product during isobutane/

Table 5. Product Distributions for Pulse Experiments^a

component	propene pulse	pulse	
		<i>trans</i> -2-butene	<i>trans</i> -2-pentene
C ₃ 's, mol %	13.8	0.0	0.0
butenes, mol %	0.0	65.2	0.0
pentenes, mol %	0.0	0.0	32.2
<i>n</i> -pentane, mol %	0.0	0.0	6.3
isopentane, mol %	7.3	1.6	15.4
C ₆ 's, mol %	6.9	1.4	3.1
C ₇ 's, mol %	53.1	0.0	2.7
C ₈ 's mol %	15.5	31.8	12.3
C ₉ ⁺ 's, mol %	3.4	0.0	28.0
TMP/DMH	4.23	6.06	4.80
2,2,4-TMP/TMP	0.61	0.24	0.60

^a USHY, $d_p = 196 \mu\text{m}$, $F = 150 \text{ mL/h}$, $T_{\text{rxn}} = 373 \text{ K}$, $T_{\text{act}} = 523 \text{ K}$, liquid phase).

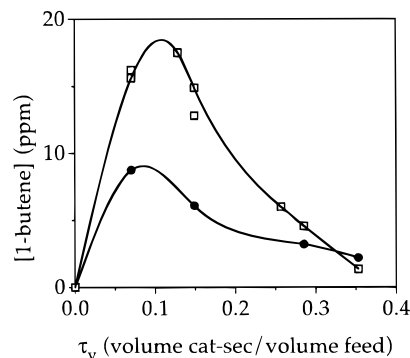
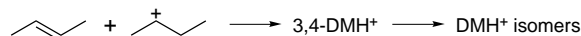


Figure 5. 1-Butene concentrations extrapolated to time zero as a function of contact time, τ_v , for $T_{\text{rxn}} = 323 \text{ K}$ (●) and 373 K (□) (USHY, $d_p = 231 \mu\text{m}$, $(\text{I/O})_0 = 890$, $T_{\text{act}} = 523 \text{ K}$).

trans-2-butene reaction as a function of contact time in the reactor. It is clear that 1-butene is both formed and consumed during alkylation and that isomerization is more pronounced at higher temperatures.

The propagation steps, through which the alkylation of isobutane with 1-butene and 2-butene proceeds, consist of the addition of an olefin to butyl cations to form C₈⁺ cations (reactions R3, R4, and R5 in Table 4), their subsequent isomerization to yield more stable C₈⁺ cations, and the abstraction of a hydride ion from isobutane by these C₈⁺ cations forming various isoocanes and a *tert*-butyl cation (reactions R6 and R7 in Table 4).

The most important addition steps in the context of alkylation catalyzed by HF and H₂SO₄ (Pines, 1981) involve reaction of *tert*-butyl cation with 1-butene and 2-butene, and these are listed in Table 4 as reactions R3 and R5, respectively. It is possible, at least in principle, to form C₈⁺ cations through the addition of a butene molecule to a *sec*-butyl cation, e.g.,



The importance of addition reactions involving *sec*-butyl cation (or lack of it) cannot be tested by the sort of experiments performed in our study. The lack of appearance of (3-)methylheptane in the reaction products indicates that the reaction of *sec*-butyl cation with 1-butene is unimportant in our experiments. Table 6, sections a and b, summarizes the time-zero values of butene conversion and TMP/DMH ratio, for liquid-phase alkylation of isobutane with *trans*-2-butene with fixed feed composition, at different contact times and feed I/O ratios. The effect of $(\text{I/O})_0$ seen in these tables lends support to the idea that DMH's may be produced by reaction of a 2-butene molecule with a *sec*-butyl cation.

Table 6. Effect of (I/O)₀ on the Time-Zero Butene Conversion (Section a) and TMP/DMH Ratio^a

τ_v^b	(I/O) ₀ = 560	(I/O) ₀ = 820	(I/O) ₀ = 3350
Section a: Butene Conversion			
0.07	0.49	0.54	0.63
0.13	0.78	0.81	0.88
0.15	0.78	0.84	0.90
Section b: TMP/DMH			
0.07	5.2	6.0	7.9
0.13	6.0	6.0	8.5
0.15	6.0	6.3	8.0

^a USHY, $d_p = 231 \mu\text{m}$, $T_{\text{rxn}} = 373 \text{ K}$, $T_{\text{act}} = 523 \text{ K}$, liquid phase.^b In units of volume of catalyst/s/volume of feed.

An increase in the concentration of butene in the feed should lead to a higher concentration of *sec*-butyl cations on the surface, thus leading to the observed drop in the TMP/DMH ratio.

Butene conversion increases with contact time, as one would expect (Table 6a). Note that the conversion also increases with feed I/O ratio, clearly demonstrating that alkylation is not strictly first order in butene concentration. Therefore, the previous analysis which relied upon the reaction being first order should be considered to be approximate and only a preliminary estimate. A more detailed kinetic analysis will be developed in the next section. Note also that the DMH fraction decreased as the contact time in the reactor was increased. Increasing the contact time increases butene conversion, thus decreasing the average concentration of butene in the reactor. Therefore, the effects of contact time and feed I/O ratio on DMH selectivity are internally consistent.

The effect of temperature on the TMP/DMH ratio shown in Table 2 can be easily rationalized at this point. Recall from Table 4 that there are two routes to DMH molecules (reactions R4 and R5) but only one route to TMP's (reaction R3). As the temperature is lowered, the extent of butene isomerization to 1-butene is lowered (see Figure 5). This results in an increase in the extent of reaction R3 and a decrease in the extent of reaction R5, serving to increase the TMP/DMH ratio. The relative importance of reactions R3 and R4 depends upon the relative surface concentrations of *tert*-butyl and *sec*-butyl cations. Since the *tert*-butyl cation is energetically more stable than the *sec*-butyl cation, it is likely that decreasing the temperature will increase the surface *tert*-butyl to *sec*-butyl cation ratio, again resulting in an increase in the TMP/DMH ratio. However, decreasing the temperature also serves to decrease the average I/O ratio over the catalyst bed. As seen in Table 6b, decreasing the I/O ratio of the feed results in a decrease in the TMP/DMH ratio. Presumably, this is due to an increase in the concentration of *sec*-butyl cations on the surface. Thus, it can be seen that as the temperature is lowered, there are two effects which increase the TMP/DMH ratio, while there is one effect which decreases the TMP/DMH ratio. The end result is a TMP/DMH vs temperature plot with a local maximum, as seen in Table 2.

Larger carbocations can form through successive addition of olefin molecules to the C_8^+ cations, an example of which is included in Table 4 as reaction R8. Such large carbocations can disproportionate (e.g., see reaction R9) to form hydrocarbon molecules and smaller carbocations which, in turn, can participate in olefin addition and/or hydride abstraction (reaction R10) reactions. This is the most likely pathway for the formation of the C_5 , C_6 , C_7 , and C_9 products listed in Tables 1 and

3 (Pines, 1981). Disproportionation to form C_2 's and C_3 's is not considered, since these products were not observed in our experiments.

It has been suggested by Kirsch et al. (1972) and Corma and Martinez (1993) that self-alkylation of isobutane may be important in alkylation over H-Y zeolites. This reaction may proceed through the deprotonation of a *tert*-butyl cation to form isobutylene (reaction R11 in Table 4), which subsequently reacts with another *tert*-butyl cation to form a C_8^+ cation (reaction R12). It is difficult to establish from our data the relative importance of isobutane self-alkylation and its alkylation with *n*-butenes. Isobutane alkylation performed using olefins other than butenes are more useful for this purpose. In our pulse experiments with 2-pentene (see Table 5), the noticeably higher concentration of C_8 hydrocarbons (when compared to the C_6 and C_7 compounds) suggests that self-alkylation may be taking place at an appreciable rate. (If the only source of C_8 hydrocarbons is disproportionation, it is not clear why the concentration of C_8 should be much different from those of C_6 and C_7 .)

To test this point further, pulse experiments were performed using propene. As expected, C_7 alkylates constitute the main products (see Table 5). The propane and propene in the product stream have been lumped together, as they were not resolved by the Petrocol DH capillary column used in our GC to separate the products. The material balance closure was found to be very good in pulse experiments with pentene. In contrast, this closure was poor in propene pulse experiments. It is plausible that appreciable amounts of C_4 compounds were formed in propene experiments, which could not be determined in our experiments. In any case, an appreciably higher level of C_8 , when compared to C_5 and C_6 compounds, was observed in propene pulse experiments as well (Table 5). Alkylation of isobutane with propene is initiated by the formation of C_3^+ cations which produce C_4^+ cations through hydride abstraction from isobutane. Successive addition of propene to a C_3^+ cation results in the formation of C_6^+ , C_9^+ , C_{12}^+ , etc., while successive addition of propene to a C_4^+ cation results in the formation of C_7^+ , C_{10}^+ , C_{13}^+ , and so on. Given that only a small amount of propene was fed to the reactor in pulse experiments, formation of large carbocations such as C_{12}^+ and C_{13}^+ is not very likely. Yet, such large cations are required if C_8 hydrocarbons were to form only by disproportionation. The presence of an appreciable amount of C_8 in the product mixture (Table 5) may, therefore, be taken as indirect evidence for the existence of another pathway for the formation of C_8 molecules.

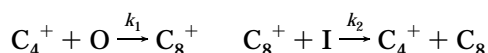
It may also be argued that self-alkylation is inevitable in pulse experiments. Alkylation is initiated when olefin first enters the reactor. The propagation and disproportionation steps continue as long as olefins remain in the reactor. As the olefins wash out of the reactor, the small carbocations (predominantly $t\text{-C}_4^+$) residing on the catalyst surface can only deprotonate, forming isoolefins which then react with other carbocations still on the surface. Thus, if $t\text{-C}_4^+$ is present on the surface and only isobutane is available in the fluid phase, the most likely set of reactions are (R11), (R12), and then (R6).

The addition of isobutylene to $t\text{-C}_4^+$ results in the formation of a tertiary carbocation. The inherent stability of such tertiary carbenium ions suggests that its isomerization will not be favorable, as a secondary

carbenium ion needs to be formed in any isomerization pathway starting from this carbocation. If we neglect isomerization, then 2,2,4-trimethylpentane will be the preferred product formed in the above set of reactions. Indeed, in propene and pentene pulse experiments, 2,2,4-TMP accounted for 60% of the trimethylpentanes formed. In the *trans*-2-butene pulse experiment, where trimethylpentanes can form through both self-alkylation and normal alkylation, only 25% of the TMP was 2,2,4-TMP (see Table 5).

Quantitative Analysis of Time-Zero Butene Conversion. Although one can write down a detailed kinetic model for alkylation on the basis of the mechanism discussed above which accounts for the selectivities to various products, estimating the large number of parameters contained in such a model is a formidable problem. The observation made earlier that the reaction is severely limited by diffusion compounds the complexity of such an endeavor. It is not difficult, however, to extract some quantitative information about the key steps involved in alkylation from the time-zero butene conversion data gathered in this study.

Clearly, the most important steps in alkylation, at least under liquid-phase conditions, are the propagation reactions (R3–R7). If one assumes that the olefin addition steps (reactions R3–R5) are treated as effectively the same reaction with rate constant k_1 and that the hydride-transfer steps (reactions R6 and R7) are likewise treated as a single reaction with rate constant k_2 , then the mechanism can be reduced to the following form:



As discussed later in a greater detail, the successive addition of olefins to carbocations, i.e., olefin polymerization, is generally believed to be the primary route to catalyst deactivation. The olefin addition reaction above is sometimes referred as a polymerization step, while the hydride-transfer reaction is denoted as the main alkylation reaction. Restricting our attention to just this set of reactions and assuming quasi steady state for the concentrations of the carbocations, the intrinsic rate of butene conversion per unit volume of catalyst can be written as

$$R_{\text{int}} = \frac{k_1 C_O [C_4^+]}{[S]_0} = \frac{k_2 C_I [C_8^+]}{[S]_0} = \frac{k_1 C_O}{1 + K(C_O/C_I)} \quad \text{kmol}/(\text{m}^3 \text{ of catalyst} \cdot \text{s})$$

where $K = k_1/k_2$, $[C_4^+]$ and $[C_8^+]$ are the concentrations of C_4^+ and C_8^+ (kmol/m³ of catalyst), $[S]_0$ is the concentration of active sites in the fresh catalyst (kmol/m³ of catalyst), and $[C_4^+] + [C_8^+] = [S]_0$. The affinity of the olefin to the surface is so high that $[H^+]$ is assumed to be small under reaction conditions. This rate expression should be combined with a description of diffusion and reaction inside a catalyst pellet to obtain the effective rate of reaction at any location in the packed bed reactor. One should then integrate the effective reaction rates over the length of the reactor to obtain the overall (time-zero) conversion of butene in the reactor. The details of this analysis are described elsewhere (Simpson, 1996).

The butene conversion data obtained from kinetic experiments performed at 373 K over USHY pellets of different diameters, feed compositions, and WHSV's

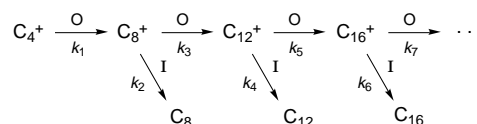
were then regressed using this equation. The best-fit values of k and K were found to be

$$k(373 \text{ K}) = \frac{k_1 D \rho_p^2}{\rho_p^2} = 1.440 \times 10^{-7} \text{ m}^2/\text{s}^2$$

$$K(373 \text{ K}) = k_1/k_2 = 3800$$

It was found that the model captured the data nicely (Simpson, 1996). A similar analysis performed with data gathered at 323 K gave $k(323 \text{ K}) = 0.870 \times 10^{-7} \text{ m}^2/\text{s}^2$ and $K(323 \text{ K}) = 8000$.

Routes to Deactivation. As was mentioned before, rapid catalyst deactivation is the most critical problem associated with solid-acid-catalyzed alkylation. The major goal of any solid acid alkylation project should be to understand how to minimize the rate of catalyst deactivation. Weitkamp and Maixner (1987) characterized the carbonaceous deposits formed on a Lanthanum-exchanged Y zeolite during alkylation at various temperatures. For a reaction temperature of 353 K, the deposit was found to be mostly paraffinic in nature with a H/C ratio of 1.8. At higher temperatures, the H/C ratio decreased, indicative of an increasing olefinic and aromatic nature to the deposit. The result that the first olefin addition rate constant (k_1) is 3 orders of magnitude larger than the first hydride-transfer rate constant (k_2) suggests that large paraffins may be formed within the catalyst via multiple olefin additions:



Disproportionation of large carbocations formed through multiple olefin addition into smaller fragments is not included in the above scheme. It seems reasonable to expect that these large carbocations adsorbed on the catalyst surface will be quite stable and will not be removed easily.

Even when an isobutane molecule succeeds in donating a hydride ion to such a bulky carbocation, steric effects should inhibit the diffusion of the resulting alkylate (C_{12} , C_{16} , etc.) out of the zeolite cavities. As the accumulation of large carbocations and alkylates in the zeolite cavities increases, the pores may effectively become blocked. Such a pore blockage can also lead to a decrease in catalytic activity with increasing time on-stream. Rapid deactivation during alkylation is also observed in other non-zeolitic solid acids where the pores are much larger. This suggests that the decline in catalytic activity is more likely to be due to loss of active sites resulting from the presence of large, adsorbed carbocations.

In our analysis of the deactivation rate data, we have truncated the above reaction sequence at C_{12}^+ and assumed that even C_{12}^+ formation results in an irreversible loss of active site. It then follows that decreasing the ratio of the rates of the second olefin addition to the first hydride transfer, $(k_3/k_2)(C_O/C_I)$, should decrease the rate of carbonaceous deposit buildup and, hence, decrease the rate of deactivation. The rate constant for the deactivation step, k_3 , has been determined from our experimental data, as described below.

Transient Reactor Modeling. In order to verify that the specified route to deactivation is consistent with experimental data, a mathematical model was con-

structured to capture the time-dependent butene conversion. As with the time-zero kinetic analysis, the experimental system was modeled as a plug flow reactor (PFR). For the purpose of numerical analysis, the PFR containing a total volume (V) of catalyst pellets was divided into M cells of equal volume so that the volume of catalyst in each cell is $V_i = V/M$. Assuming each cell to be well mixed,

$$F([O]_i - [O]_{i-1}) + \frac{V_i \epsilon}{1 - \epsilon} \frac{d[O]_i}{dt} + \frac{6V_i}{d_p} D \left(\frac{\partial C_O}{\partial r} \right)_{r=d_p/2} = 0, \quad i = 1, 2, \dots, M \quad (1)$$

where C_O denotes olefin concentration inside the pellet. $[O]_i$ and $[O]_{i-1}$ denote concentrations in the bulk fluid phase of cells i and $i - 1$, respectively.

Since the isobutane/butene alkylation reaction has been demonstrated to be severely diffusion-limited, it is necessary to solve for intraparticle concentration profiles. The catalyst deactivates during the reaction, necessitating material balances for both butene and the number of active sites. The butene material balance can be written as follows, assuming spherical catalyst pellets:

$$\epsilon_p \frac{\partial C_O}{\partial t} = \frac{D}{r^2} \frac{\partial}{\partial r} \left(r^2 \frac{\partial C_O}{\partial r} \right) - R \quad (2)$$

In eq 2, R is the rate of butene consumption per unit volume of catalyst. To allow for the deactivation of acid sites through accumulation of carbonaceous deposit, it is written as

$$R = \theta R_{\text{int}} = \frac{\theta k_1 C_O}{1 + K(C_O/C_I)} \quad \text{kmol of butene}/(\text{m}^3 \cdot \text{s}) \quad (3)$$

where $\theta = \theta(r, t)$ is the fraction of acid sites which are still active. The boundary and initial conditions needed to solve the olefin material balance are

$$\begin{aligned} \frac{\partial C_O}{\partial r} &= 0 \quad \text{at } r = 0, t > 0; \\ C_O &= [O]_i \quad \text{at } r = d_p/2, t > 0; \\ C_O(r) &= C_{\text{init}}(r), \quad 0 < r < d_p/2, t = 0 \end{aligned} \quad (4)$$

where C_{init} is a given initial profile of olefin concentration inside the pellet.

Assuming the rate of deactivation is proportional to the rate of C_{12}^+ formation, it can be written as

$$[S]_0 \frac{d\theta}{dt} = - \frac{k_3 K(C_O/C_I) C_O \theta}{1 + K(C_O/C_I)} \quad (5)$$

In the current study, simulations have been performed assuming that at $t = 0$, θ is unity throughout the catalyst pellets in the entire reactor.

The numerical scheme used to solve eqs 1–5 is discussed in detail elsewhere (Simpson, 1996). The values assigned for some of the dimensional parameters appearing in the model are as follows: $\epsilon = 0.50$; $\epsilon_p = 0.75$; $D = 10^{-10} \text{ m}^2/\text{s}$; $\rho_p = 1100 \text{ kg/m}^3$; $\rho_f = 550 \text{ kg/m}^3$.

In order to determine how many cells are needed to accurately emulate the performance of a PFR for this reaction/catalyst, the deactivation rate constant, k_3 , was set to zero and the steady-state version of the reactor model was solved, varying the number of cells, M , until the conversion became essentially independent of M .

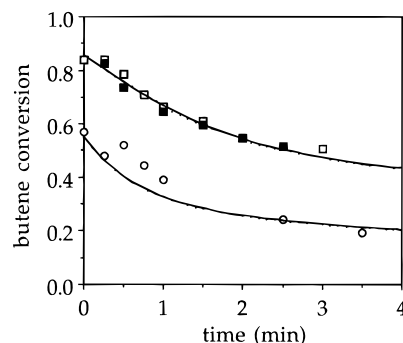


Figure 6. Fit of transient butene conversion profile to reactor model for $\tau_r = 0.07 \text{ s}$ (○) and 0.15 s (□, ■) ($d_p = 231 \mu\text{m}$, $(I/O)_0 = 850$, $T_{\text{rxn}} = 373 \text{ K}$, $T_{\text{act}} = 523 \text{ K}$).

This sort of analysis was repeated for several different operating conditions, and it was determined that 25 cells were sufficient to emulate a PFR for this reaction satisfactorily. Therefore, M has been set to 25. Such steady-state simulations were also used to ascertain that the reactor model, with the assumed/estimated parameter values listed above, satisfactorily reproduces the time-zero kinetic data determined via extrapolation (Simpson, 1996).

Computations were performed next allowing for catalyst deactivation. The acidity of USHY as measured by $\text{NH}_3\text{-TPD}$ is 1.1 mmol/g , which translates to a value of 1.2 kmol/m^3 (Simpson, 1996). Using this value as an estimate of $[S]_0$, the value of k_3 was estimated in order to produce a reasonable fit of the transient experimental data. Several different initial conditions were explored, and it was found that the concentration profiles rapidly evolved to the steady-state solution discussed above (with deactivation step turned off). As shown in Figure 6, a k_3 value of 8.3 s^{-1} fits the experimental data adequately over a range of 4 min. In these liquid-phase alkylation experiments, the feed I/O ratio was approximately 850, the reaction temperature was 373 K , and the effluent sampling was done on-line.

It is interesting to observe that the rate constant for the deactivation reaction is smaller than that for the addition of an olefin to a C_4^+ , namely, k_1 , by 3 orders of magnitude. It is difficult to pinpoint a reason for this difference. It is possible that the carbocation becomes less active as the number of carbon atoms increases (assuming, of course, that the same type of carbocations are being compared, such as a tertiary cation). It is also possible that the olefin addition to a C_8^+ is more sterically hindered than the addition to a C_4^+ .

It is also of interest to compare k_3 and k_2 . It was estimated using the time-zero kinetic analysis that k_2 (373 K) is 1.5 s^{-1} . Therefore, k_3 is 5.5 times larger than k_2 . Thus, the addition of an olefin to a C_8^+ is intrinsically more favorable than a hydride abstraction reaction. Denoting the rate of olefin addition to a C_8^+ by R_3 and the rate of hydride abstraction (from an isobutane by a C_8^+) by R_2 ,

$$R_2/R_3 = \frac{k_2 C_I}{k_3 C_O} = 0.18(C_I/C_O) \quad (6)$$

As the feed I/O ratios in the experiments described herein were typically around 1000, it can be concluded that each active site accessed by butene (recall that the reaction is limited severely by intraparticle diffusion) produced roughly several hundred molecules of alkylate before being deactivated. In contrast, if one exposes the

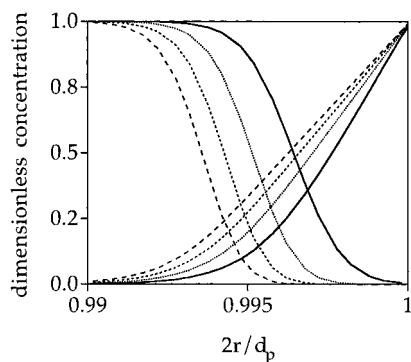


Figure 7. Computed intraparticle butene and active site concentration profiles at 6 s (—), 60 s (···), 120 s (---), and 240 s (- · -) time on stream near the upstream end of the reactor ($k_1 = 5760 \text{ s}^{-1}$, $k_2 = 1.5 \text{ s}^{-1}$, $k_3 = 8.3 \text{ s}^{-1}$, $d_p = 231 \mu\text{m}$, $\tau_v = 0.7$ (volume of catalyst/s/volume of feed), $(I/O)_0 = 810$). The results plotted here are for the first cell of a 25-cell model for the PFR.

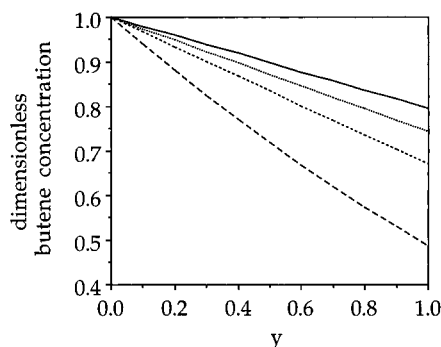


Figure 8. Computed bulk butene concentration profiles in reactor at 6 s (—), 60 s (---), 120 s (···), and 240 s (- · -) time on stream (see caption of Figure 7 for parameter values).

fresh catalyst to a feed with an I/O ratio in the range of 5–15 (which is typical of industrial alkylation conditions), only a few molecules of alkylate will be produced by each acid site before being deactivated. Note that the problem of severe intraparticle diffusion limitations prevents the acid sites in the interior of the pellet from participating in the alkylation reaction. Thus, the effective turnover number based on the total number of Brönsted acid sites in the reactor will be smaller than the above-mentioned numbers by a factor approximately equal to the Thiele modulus. Therefore, even with I/O ratios as high as 1000, the effective turnover number for the pellets used in our study is only in the range of 1–10.

Typical intraparticle butene and active site concentration profiles for a particle near the reactor entrance are given in Figure 7. As seen here, a deactivation front moves progressively deeper into the catalyst with increasing time on stream. Note that the results are shown for a very thin shell of catalyst near the external surface. For the same set of conditions as in Figure 7, the bulk concentration profiles in the reactor at various times on stream are shown in Figure 8. The abscissa in this figure, y , is simply the dimensionless axial position within the reactor.

It is readily obvious from the form of the mathematical model employed to analyze the kinetic data that a high value of k_3/k_2 is the cause of the unacceptably high rate of catalyst deactivation. It is interesting to explore the extent to which the catalyst performance can be improved by changing the ratio of the rate constants k_3/k_2 or the feed composition, $(I/O)_0$. As k_1 and k_3 represent rate constants for similar reaction events, namely, olefin addition to carbocations, it seems reason-

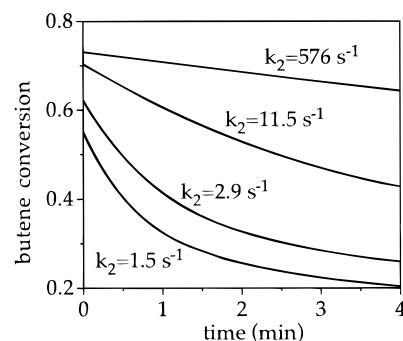


Figure 9. Computed butene conversion as a function of time for various k_2 values (see caption of Figure 7 for values of all other parameters).

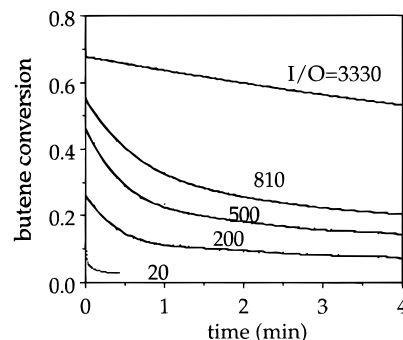


Figure 10. Computed butene conversion as a function of time for various feed I/O ratios (see caption of Figure 7 for values of all other parameters).

able to expect that the ratio k_1/k_3 will not vary significantly with changes in reaction conditions such as temperature or with simple changes in catalyst formulation. We have therefore kept the ratio k_1/k_3 fixed in the examples presented below. For fixed values of k_1 and k_3 , the conversion profiles have been calculated for various values of k_2 ; see Figure 9. It can be seen that both the initial conversion and the resistance to catalyst deactivation are improved by increasing k_2 .

The effect of $(I/O)_0$ on butene conversion is shown in Figure 10. It is clear that decreasing $(I/O)_0$ increases the rate of deactivation. When $(I/O)_0$ is lowered to 20, deactivation occurs in a matter of seconds. This was, indeed, the case when experiments were attempted in our laboratory with low I/O ratios.

Interestingly, if the conversion is plotted vs the cumulative moles of butene contacted with the catalyst rather than vs the time on stream, then it can be shown that simulations with different k_3/k_2 and $(I/O)_0$ but with identical $(k_3/k_2)(O/I)_0$ have results that collapse onto a single curve (see Figure 11). Such a result is easily rationalized by casting the model equations in dimensionless form (Simpson, 1996). Thus, there is an inverse relationship between k_3/k_2 and $(I/O)_0$. Lowering the value of k_3/k_2 allows one to obtain a given level of reactor performance using a lower $(I/O)_0$, which is desirable from a practical point of view.

One can readily see that, from a process design standpoint, a once-through PFR such as the one used in our experiments is hardly desirable. It is more advantageous to use a CSTR or a PFR with a distributed feed of the olefins so that the I/O ratios at various locations inside the reactor are kept as low as possible. This should slow down the rate of catalyst deactivation and improve catalyst utilization.

Pulsed Flow Alkylation. A limited set of experiments in which the feed composition was periodically

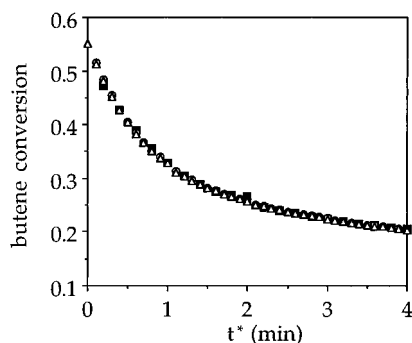


Figure 11. Computed butene conversion as a function of time, $t^* = t(I/O)_0/810$. $k_1 = 5760 \text{ s}^{-1}$, $k_3 = 8.3 \text{ s}^{-1}$, $d_p = 231 \text{ }\mu\text{m}$, $\tau_v = 0.07$ (volume of catalyst-s/volume of feed). Results are shown for three different values of $(I/O)_0 = 81$ (\circ), 405 (\blacksquare), 810 (\triangle). The value of k_2 is adjusted so that $(k_3/k_2)(O/I)_0 = 0.00676$ for all cases.

pulsed were performed. Such experiments were motivated by the kinetic analysis described earlier in this paper. Recall that the key steps in alkylation are olefin addition to butyl cations (reactions R3–R5), hydride transfer to octyl cations (reactions R6 and R7), and olefin addition to octyl cations (reaction R8). When the fluid phase in contact with the catalyst contains both isobutane and olefin, all of the three steps occur simultaneously and catalyst decay is inevitable. It is instructive to ask whether one can devise a scheme for contacting the reactants with the catalyst which, at least theoretically, can mitigate or even eliminate altogether the deactivation step (reaction R8).

Such a *hypothetical* scheme can, indeed, be imagined. Suppose the USHY is first contacted with a stream containing isobutane and a very small amount of 2-butene. The olefin adsorbs onto the acid site, producing *sec*-butyl cations. These *sec*-butyl cations, in turn, will abstract a hydride ion from isobutane, forming *n*-butane and a *tert*-butyl cation. This way, butyl cations have been placed on each acid site. Then the catalyst is contacted with just enough 2-butene so that one butene molecule reacts with each C_4^+ cation, producing a C_8^+ (reaction R4–R6). In this hypothetical scheme, no additional butene is available to react further with C_8^+ to produce C_{12}^+ , etc. Thus, the only reaction possible for C_8^+ is the hydride abstraction step (reaction R6 and R7), as isobutane is the only reactant available. Enough time is provided for this step to be completed so that all of the C_8^+ has been converted to C_4^+ . Then the process of dosing the catalyst bed with butene is repeated. By cycling through this process, C_8 alkylates may be produced in the absence of catalyst deactivation! In this scheme, isomerization of butene will be suppressed, as there will be no *sec*-butyl cations in the catalyst at any time after the first butene pulse. Recall that 1-butene reacting with a *tert*-butyl cation is the dominant route to produce DMH^+ , while 2-butene reacting with *tert*-butyl cations leads to TMP^+ . The pulsed feed scheme, thus, should lead only to the formation of TMP 's!

This extent of reaction control is, of course, very hard to achieve in practice, as such a perfect decoupling of the reaction steps cannot be engineered. The fact that the reaction is severely limited by intraparticle diffusional resistance further compounds the problem. Nevertheless, it should be feasible to verify whether an appreciable change in the rate of deactivation and the TMP/DMH ratio can be achieved by injecting butene into the reactor as periodic pulses.

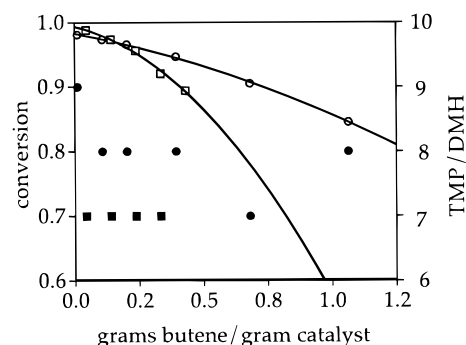


Figure 12. Comparison of pulsed flow and steady flow modes of operation (USHY, $d_p = 231 \text{ }\mu\text{m}$, $WHSV \approx 5400 \text{ h}^{-1}$, $(I/O)_{0,avg} \approx 890$, pulse period = 5 s, $T_{rxn} = 373 \text{ K}$, $T_{act} = 523 \text{ K}$). Butene conversion (\circ) pulsed, (\square) steady flow. TMP/DMH ratio (\bullet) pulsed, (\blacksquare) steady flow.

USHY was again used as a model catalyst to study the effect of pulsing the flow on the alkylation catalysis characteristics. In order to understand how the size of the pulse relative to the mass of the catalyst affects the conversion and selectivity, a series of experiments were performed with varying R values. R is defined as the ratio of the amount of butene in a single pulse (N_0) to the amount of acid sites in the catalyst (N_a). It was assumed that N_a is equal to the amount of framework Al in the catalyst, which can be accessed by the butene molecules. This density was estimated to be 2.1 mmol/g based upon a framework Si/Al ratio of 6.9. Since the reaction is severely diffusion limited, only an outer shell of each catalyst pellet can participate in the reaction. The penetration depth, δ_c , was estimated using $\delta_c = (D\tau)^{1/2}$, where τ is a suitable characteristic time. In the analysis presented here, τ is taken to be $\epsilon\tau_v/(1 - \epsilon)$. The value for N_0 was determined based upon the known 5% concentration of *trans*-2-butene in the butene/isobutane mixture and the known sample loop volumes.

Whether the operation of an alkylation reactor in a pulsed flow mode is beneficial or not can be evaluated by comparing results obtained under pulsed flow mode with data from experiments with a steady feed concentration. One then has to confront the issue of what constitutes a fair comparison. If the pulsed flow experimental results are compared with data from experiments with a steady feed concentration of 5% *trans*-2-butene, it is immediately found that the pulsed flow mode is far superior in both the total amount of butene that can be converted and the alkylate quality. One can argue, however, that this is not a fair comparison and that it is more appropriate to compare pulsed flow data with steady feed concentration experiments having the same *average* $(I/O)_0$ value.

Making such a comparison, the advantage of pulsed flow relative to steady flow can be seen in Figure 12, which is representative of several experiments performed in the present study. This figure shows the time-dependent conversion and TMP/DMH ratio data for experiments involving steady flow and pulsed flow (pulse period of 5 s) as a function of grams of butene contacted per gram of catalyst. Even though the initial extent of butene conversion is slightly less for the pulsed experiments, the resistance to deactivation and the TMP/DMH ratio appear to be improved.

Issues on Catalyst Design. The most obvious changes which can be made in the formulation of the catalyst are the *physical* changes. As the alkylation reaction under liquid-phase conditions is severely limited by intraparticle diffusion, it is hardly effective to

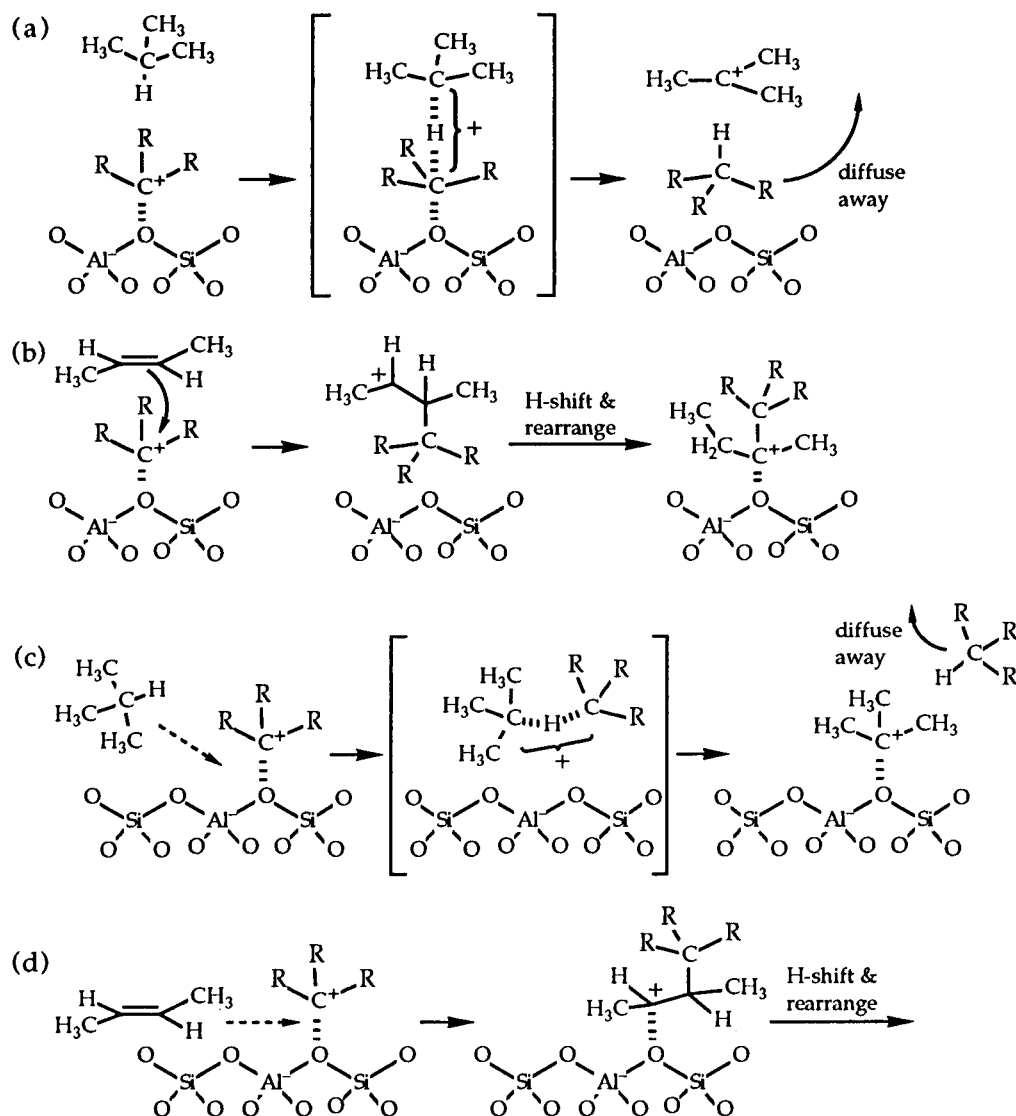


Figure 13. Trajectories of approach of isobutane or 2-butene to a carbocation attached to an acidic site on a zeolite: backside attack by isobutane (a) and 2-butene (b); edge-on attack by isobutane (c) and 2-butene (d).

place the acid sites uniformly throughout the pellet. It is more sensible to locate the acid sites exclusively near the external surface of the pellet. Actually, one can argue that it would be more desirable to place the active (acid) sites as a thin shell at a small distance (a few microns) away from the external surface so that intraparticle diffusional resistance continues to play a small role. By doing so, butene (the stoichiometrically limiting reactant) is forced to diffuse through a finite distance before reaching the acid sites—so that the concentration of olefin in the vicinity of the acid sites can be made appreciably smaller than that in the bulk fluid phase outside the pellet (i.e., $(I/O)_{\text{bulk}} \ll (I/O)_{\text{near the acid sites}}$). This should enhance the selectivity to TMP and slow down the rate of catalyst deactivation.

It is difficult to make concrete recommendations on chemical changes in the catalyst which will mitigate the deactivation problems. It is clear that the key is to develop a strategy for increasing the intrinsic rate of hydride transfer relative to olefin addition to a C_8^+ (increase k_2/k_3). We speculate that, in the various solid acid catalysts that have been tried in the past, the hydride abstraction step is sterically more hindered than the olefin addition step. This is illustrated in a figure showing schematically the events at an acid site on a zeolite lattice. There are two possible trajectories

for the approach of either isobutane or 2-butene to a carbocation attached to an acidic site: backside attack or edge-on attack. Backside attacks of isobutane and 2-butene are illustrated in Figure 13a and 13b, respectively. The approach of the tertiary C–H group to the tertiary cation on the surface is sterically very difficult, but the approach of 2-butene, a secondary olefin, is less so. Edge-on attacks of isobutane and 2-butene are illustrated in Figure 13c and 13d. Here, each molecule must approach by sliding along the surface of the zeolite. The olefin can adopt an orientation parallel to the surface (at a distance of approximately 3.2 Å—the sum of the van der Waals radii of carbon and oxygen) and easily slide between the cation and the zeolite framework to permit interaction between the π -system of the olefin and the carbocation. In the likely orientation for hydride abstraction from the isobutane, the C–H bond must be pointing away from the surface. However, because of the tripod of methyl groups, the tertiary carbon is held at least 4.1 Å away from the surface and cannot easily move into position for hydride abstraction. Whatever the trajectory, the approach of a tertiary carbon atom to a surface carbocation, close enough for hydride abstraction, is more sterically demanding than the approach of a secondary olefin. At least for the case of edge-on attack, the steric hindrance to hydride

abstraction will be relieved by attaching the acid group to a tether and extending it away from a support surface (to which the other end of the tether is attached). By disencumbering the acid, both the hydride abstraction step and olefin addition will likely be accelerated, but the hydride abstraction should show the greater increase in rate. If, on the other hand, backside attack predominates, then tethering the acid group should have a less pronounced effect on the reaction rates. However, the long tethered acid, now removed from the surface, should be less susceptible to fouling by the adsorption of higher molecular weight species regardless of the trajectory of approach of the alkanes and olefins. It would be interesting to verify whether such tethered acids do manifest markedly lower rates of deactivation.

Summary

The mechanism of alkylation over USHY is similar to that known for the liquid-acid-catalyzed reaction. Though this mechanism involves several different fundamental reactions, the reaction kinetics can be analyzed on the basis of two key steps—olefin addition to a C_4^+ and hydride transfer to a C_8^+ . The reaction was found to be severely limited by intraparticle diffusion when using liquid-phase reaction conditions. Placing the acid sites in the vicinity of the pellet's external surface is therefore desirable. Switching to the vapor phase resulted in significantly less diffusional control, but the product selectivity suffered dramatically.

A sequential, site-coverage deactivation model captures adequately the transient conversion data obtained. The rate constant for addition of an olefin to a C_8^+ , k_3 , was found to be much smaller than that for adding the same olefin to a C_4^+ , k_1 . It was also found that the ratio of k_3 to the rate constant for hydride transfer to a C_8^+ , k_2 , is too large and that this is responsible for the rapid deactivation of the catalyst. It is suggested that the hydride-transfer step may be sterically hindered.

As very high feed I/O ratios help minimize the rate of catalyst deactivation, a CSTR and a PFR with a distributed feed of olefin represent more desirable reactor configurations than a standard PFR.

The kinetic model for alkylation and catalyst deactivation suggest that a time-varying feed butene concentration may serve to improve the selectivity toward TMP's and to reduce the rate of catalyst deactivation. These effects were, indeed, verified.

Acknowledgment

We gratefully acknowledge advice on pitfalls in alkylation experiments provided by Dr. Weldon Bell (Mobil), valuable discussions with Prof. Jay Benziger, Prof. Robert A. Pascal, Jr., and Mr. Amer Akhras (Princeton University), and financial support provided by the National Science Foundation (CTS-9216699).

Nomenclature

$C_{\text{init}}(t)$ = initial intraparticle olefin concentration profile (kmol/m³ of catalyst)
 C_i , C_o = intraparticle concentration of isobutane and olefin, respectively (kmol/m³ of catalyst)
 $[C_4^+]$, $[C_8^+]$, $[C_{12}^+]$ = concentration of C_8^+ , C_8^+ , and C_{12}^+ , respectively (kmol/m³ of catalyst)
 D = effective diffusivity in catalyst particles (m²/s)
 d_p = average catalyst particle diameter (m)
 F = volumetric flow rate of feed (m³/s)
 I/O = molar isobutane to olefin (butene) ratio
 $(I/O)_0$ = molar feed isobutane to olefin (butene) ratio
 k = grouped kinetic parameter ($k = k_1 D \rho_i^2 / \rho_p^2$, m²/s²)

K = ratio of kinetic model rate constants ($K = k_1/k_2$)
 k_{app} = apparent first-order rate constant, volume basis (volume of feed/volume of catalyst·s)
 k_1 , k_2 , k_3 = kinetic model rate constants (1/s)
 M = number of cells used to simulate a plug flow reactor
 N_a = moles of acid sites in catalyst bed available for alkylation (kmol)
 N_0 = amount of butene per pulse (kmol)
 $[O]$ = bulk olefin concentration (kmol/m³ of catalyst)
 $[O]_i$ = bulk olefin concentration in cell i (kmol/m³ of catalyst)
 $[O]_{0,\text{avg}}$ = time-averaged feed olefin concentration (kmol/m³ of catalyst)
 $(O/I)_0$ = molar feed olefin to isobutane ratio
 r = radial position within catalyst pellet (m)
 R = rate of butene consumption in catalyst pellets (kmol/m³ of catalyst·s)
 R = ratio of moles of butene in pulse to moles of acid sites in catalyst bed
 R_2 = intrinsic rate of hydride transfer (kmol/m³ of catalyst·s)
 R_3 = intrinsic rate of the second olefin addition to form C_{12}^+ (kmol/m³ of catalyst·s)
 R_{int} , R_{obs} = intrinsic and observed rates of butene consumption, respectively (kmol/m³ of catalyst·s)
 $[S]_0$ = initial concentration of active sites (kmol/m³ of catalyst)
 Si/Al = framework Si/Al ratio of zeolite
 t^* = scaled time on stream (min); see Figure 11
 T_{act} = temperature of activation (K)
 T_{rxn} = temperature of reaction (K)
 TOS = time on stream (min)
 TMP/DMH = molar trimethylpentane-to-dimethylhexane ratio
 $(\text{TMP/DMH})_0$ = time-zero molar trimethylpentane-to-dimethylhexane ratio
 V = total volume of catalyst pellets (m³)
 V_i = volume of catalyst per cell (m³)
 WHSV = weight hourly space velocity (h⁻¹)
 x = time-zero butene conversion
 y = dimensionless axial position along reactor

Greek Symbols

δ_c = depth of active catalyst layer (m)
 ϵ = reactor void fraction
 ϵ_p = porosity of catalyst pellets
 ϕ = Thiele modulus
 η = effectiveness factor
 ρ_p = catalyst pellet density (kg/m³)
 ρ_f = density of feed liquid (kg/m³)
 θ = fraction of the sites that are active
 τ = time scale for diffusion (s)
 τ_v = volume-based contact time (m³ of catalyst·s/volume of feed)

Literature Cited

- Albright, L. F. Mechanism for Alkylation of Isobutane with Light Olefins. In *Industrial and Laboratory Alkylations*; Albright, L. F., Goldsby, A. R., Eds.; ACS Symposium Series 55; American Chemical Society: Washington, DC, 1977; Chapter 8.
- Albright, L. F. H_2SO_4 , HF processes compared, and new technologies revealed. *Oil Gas J.* **1990** (Nov 26), 70.
- Chu, Y. F.; Chester, A. W. Reactions of isobutane with butene over zeolite catalysts. *Zeolites* **1986**, 6, 195.
- Corma, A.; Martinez, A. Chemistry, Catalysts, and Processes for Isoparaffin-Olefin Alkylation: Actual Situation and Future Trends. *Catal. Rev.-Sci. Eng.* **1993**, 35, 483.
- Corma, A.; Martinez, A.; Martinez, C. Isobutane/2-Butene Alkylation on Ultrastable Y Zeolites: Influence of Zeolite Unit Cell Size. *J. Catal.* **1994a**, 146, 185.
- Corma, A.; Juan-Rajadell, M. I.; Lopez-Nieto, J. M.; Martinez, A.; Martinez, C. A. comparative study of $\text{O}_4^{2-}/\text{ZrO}_2$ and zeolite beta as catalysts for the isomerization of n-butane and the alkylation of isobutane with 2-butene. *App. Catal. A: Gen.* **1994b**, 111, 175.

- Corma, A.; Gomez, A.; Martinez, A. Zeolite beta as a catalyst for alkylation of isobutane with 2-butene. Influence of synthesis conditions and process variables. *App. Catal. A: Gen.* **1994c**, *119*, 83.
- Corma, A.; Martinez, A.; Martinez, C. Influence of Process Variables on the Continuous Alkylation of Isobutane with 2-Butene on Superacid Sulfated Zirconia Catalysts. *J. Catal.* **1994d**, *149*, 52.
- Fthenakis, V. M. *Prevention and Control of Accidental Releases of Hazardous Gases*; Van Nostrand Reinhold: New York, 1993; p 267.
- Gates, B. C. *Catalytic Chemistry*; John Wiley & Sons: New York, 1992; pp 271–2.
- Grayson, M., Ed. *Kirk–Othmer Encyclopedia of Chemical Technology*; John Wiley and Sons: New York, 1978; p 50.
- Guo, C.; Yao, S.; Cao, J.; Qian, Z. Alkylation of isobutane with butenes over solid superacids, $\text{SO}_4^{2-}/\text{ZrO}_2$ and $\text{SO}_4^{2-}/\text{TiO}_2$. *App. Catal. A: Gen.* **1994a**, *107*, 229.
- Guo, C.; Liao, S.; Qian, Z.; Tanabe, K. Alkylation of isobutane with butenes over solid acid catalysts. *App. Catal. A: Gen.* **1994b**, *107*, 239.
- Kirsch, F. W.; Potts, J. D.; Barmby, D. S. Isoparaffin–Olefin Alkylations with Crystalline Aluminosilicates. I. Early Studies–C4–Olefins. *J. Catal.* **1972**, *27*, 142.
- McClure, J. D.; Brandenberger, S. G. Hydrocarbon Conversion Process using a Supported Perfluorinated Polymer Catalyst. U.S. Patent 4,038,213, 1977.
- Okuhara, T.; Yamashita, M.; Na, K.; Misono, M. Alkylation of Isobutane with Butenes Catalyzed by a Cesium Hydrogen Salt of 12-Tunstophosphoric Acid. *Chem. Lett.* **1994**, 1451.
- Pines, H. *The Chemistry of Catalytic Hydrocarbon Conversions*; Academic: New York, 1981; p 50.
- Rose, J. W., Cooper, J. R., Eds. *Technical Data on Fuel*; John Wiley and Sons: New York, 1977; p 286.
- Simpson, M. F. The Zeolite-Catalyzed Alkylation of Isobutane with Butene. Ph.D. Dissertation, Princeton University, Princeton, NJ, 1996.
- Simpson, M.; Wei, J.; Sundaresan, S. Kinetics of Zeolitic Solid-acid Catalyzed Alkylation of Isobutane with 2-Butene. In *Green Chemistry: Designing Chemistry for the Environment*; ACS Symposium Series 626; American Chemical Society: Washington, DC, 1996; p 105.
- Stöcker, M.; Mostad, H.; Rørvik, T. Isobutane/2-butene alkylation on faujasite-type zeolites (H EMT and H FAU). *Catal. Lett.* **1994**, *28*, 203.
- Ward, J. The Nature of Active Sites on Zeolites I. The Decationated Y Zeolite. *J. Catal.* **1967**, *9*, 225.
- Weisz, P. B.; Prater, C. D. Interpretation of Measurements in Experimental Catalysis. *Adv. Catal.* **1954**, *6*, 143.
- Weitkamp, J. Isobutane/Butene Alkylation on Cerium Exchanged X and Y Zeolites. In *Catalysis by Zeolites*; Imelik, B., et al., Eds.; Elsevier: Amsterdam, 1980; pp 65–75.
- Weitkamp, J.; Maixner, S. Isobutane/butene alkylation on a LaNaY zeolite. Characterization of carbonaceous deposits by CP/MAS 13C n.m.r. spectroscopy. *Zeolites* **1987**, *7*, 6.
- Weitkamp, J.; Jacobs, P. A. Isobutane/1-Butene Alkylation on Pentasil-Type Zeolite Catalysts. In *New Frontiers in Catalysis*; Guzzi, L., et al., Eds.; Elsevier: Amsterdam, 1993; pp 1735–1738.

Received for review March 27, 1996

Revised manuscript received June 5, 1996

Accepted August 2, 1996[®]

IE960172Y

[®] Abstract published in *Advance ACS Abstracts*, October 1, 1996.